

Polyhedron Transformation toward Stable Narrow-Band Green Phosphors for Wide-Color-Gamut Liquid Crystal Display

Hongxu Liao, Ming Zhao, Yayun Zhou, Maxim S. Molochev, Quanlin Liu, Qinyuan Zhang, and Zhiguo Xia*

A robust and stable narrow-band green emitter is recognized as a key enabler for wide-color-gamut liquid crystal display (LCD) backlights. Herein, an emerging rare earth silicate phosphor, $\text{RbNa}(\text{Li}_3\text{SiO}_4)_2\text{:Eu}^{2+}$ (RN:Eu²⁺) with exceptional optical properties and excellent thermal stability, is reported. The resulting RN:Eu²⁺ phosphor presents a narrow green emission band centered at 523 nm with a full width at half maximum of 41 nm and excellent thermal stability (102% @ 425 K of the integrated emission intensity at 300 K). RN:Eu²⁺ also shows a high quantum efficiency, an improved chemical stability, and a reduced Stokes shift owing to the modified local environment, in which $[\text{NaO}_8]$ cubes replace $[\text{LiO}_4]$ squares in $\text{RbLi}(\text{Li}_3\text{SiO}_4)_2\text{:Eu}^{2+}$ via polyhedron transformation. White light-emitting diode (wLED) devices with a wide color gamut (113% National Television System Committee (NTSC)) and high luminous efficacy (111.08 lm W⁻¹) are obtained by combining RN:Eu²⁺ as the green emitter, $\text{K}_2\text{SiF}_6\text{:Mn}^{4+}$ as the red emitter, and blue-emitting InGaN chips. Using these wLEDs as backlights, a prototype 20.5 in. LCD screen is fabricated, demonstrating the bright future of stable RN:Eu²⁺ for wide-color-gamut LCD backlight application.

1. Introduction

Display technology has been deeply and widely integrated into our daily lives, and its application ranges from smartphones, tablets, and computers to large-screen television (TV), versatile flexible screen, and data projectors.^[1] Presently, the technique on solid-state light-emitting diodes (LEDs) used as backlights in liquid crystal displays (LCDs) has become the driving source in the display market, and organic light-emitting diodes (OLEDs), quantum dot LEDs (QLEDs, electroluminescence), and micro LEDs can also play different roles in the respective fields.^[2] From the evaluation of technology maturity, cost, and durability, there is no doubt that LCD technique dominates the display field.^[1b,3] However, the traditional backlight units of LCD cannot satisfy the need of wide-color-gamut display. As consumers are more faithful to natural colors, it is necessary to

develop wide-color-gamut backlights for LCDs.

Presently, there are three kinds of backlights for LCDs: (i) multichip white light-emitting diodes (wLEDs), (ii) quantum dots light-emitting diodes (QD-LEDs, photoluminescence), and (iii) phosphor-converted light-emitting diodes (pc-LEDs). Multichip wLEDs and QD-LEDs show excellent color performance and tuning abilities. However, multichip wLEDs, which comprise red-, green-, and blue-emitting chips, suffer from different degradation rates of red/green/blue LEDs, low efficiency of green chips (the “green gap”), and complicated chip-driven system that will lead to a high cost.^[4] These drawbacks limit the application of multichip wLEDs. Photoluminescent QD-LEDs have shown great potentials for next-generation display due to the narrow-band emission.^[5] However, it is difficult to maintain the initial optical properties during device fabrication and long-term operation; moreover, the price of QD-LED display devices is only affordable to few consumers. Unlike multichip LEDs and QD-LEDs, pc-LEDs are mostly used due to their high efficiency, cost effectiveness, and robustness. To date, in the state-of-the-art white LEDs, the combination of green $\beta\text{-SiAlON:Eu}^{2+}$, red $\text{K}_2\text{SiF}_6\text{:Mn}^{4+}$ (KSF:Mn⁴⁺) phosphors, and blue InGaN chip is considered as the optimum backlight for LCDs.^[4]

As a successful commercial narrow-band green-emitting phosphor, $\beta\text{-SiAlON:Eu}^{2+}$ with the emission peaking at 540 nm and a full width at half maximum (FWHM) of 54 nm assists pc-wLEDs get a larger color gamut (>90% National Television


H. X. Liao, M. Zhao, Prof. Q. L. Liu, Prof. Z. G. Xia
The Beijing Municipal Key Laboratory of New Energy Materials
and Technologies
School of Materials Sciences and Engineering
University of Science and Technology Beijing
Beijing 100083, P. R. China
E-mail: xiazg@ustb.edu.cn, xiazg@scut.edu.cn

Y. Y. Zhou, Prof. Q. Y. Zhang, Prof. Z. G. Xia
State Key Laboratory of Luminescent Materials and Devices
and Guangdong Provincial Key Laboratory of Fiber Laser Materials
and Applied Techniques
South China University of Technology
Guangzhou 510641, P.R. China

Prof. M. S. Molochev
Laboratory of Crystal Physics
Kirensky Institute of Physics
Federal Research Center KSC SB RAS
Krasnoyarsk 660036, Russia

Prof. M. S. Molochev
Department of Engineering Physics and Radioelectronics
Siberian Federal University
Krasnoyarsk 660041, Russia

Prof. M. S. Molochev
Department of Physics
Far Eastern State Transport University
Khabarovsk 680021, Russia

 The ORCID identification number(s) for the author(s) of this article can be found under <https://doi.org/10.1002/adfm.201901988>.

DOI: 10.1002/adfm.201901988

System Committee (NTSC)) than the traditional cold cathode fluorescence lamps (CCFLs, $\approx 72\%$ NTSC).^[6] However, the unsatisfactory FWHM and peak position of β -SiAlON:Eu²⁺ limit the maximum color space of wLEDs. Accordingly, Mn²⁺-based narrow-band green phosphors, such as γ -AlON:Mn²⁺, Mg²⁺, and Sr₂MgAl₂₂O₃₆:Mn²⁺, have been recently reported and show potential in wLED backlight application.^[7] But the poor quantum efficiency (QE) and long lifetime values are not suitable for LCD application. Therefore, new green phosphors with narrow-emission band, proper peak, high quantum efficiency, and short decay time are urgently needed to overcome the bottle neck of the wide-color-gamut LCD technique.

Recently, we proposed a useful strategy on the learning from the mineral structure to develop the potential host lattices for emerging wLEDs phosphors.^[8] By screening compounds that belong to UCr₄C₄-related type structure with a highly condensed and rigid framework, several narrow-band phosphors, including RbNa₃(Li₃SiO₄)₄:Eu²⁺, RbLi(Li₃SiO₄)₂:Eu²⁺ (RLSO:Eu²⁺), RbNa₂K(Li₃SiO₄)₄:Eu²⁺, NaLi₃SiO₄:Eu²⁺, and NaK₇(Li₃SiO₄)₈:Eu²⁺, were developed by our group and other groups.^[8c,9] And all these compounds have been also given in the patent WO 2018/029304A1 issued by OSRAM Opto Semiconductors.^[10] Among them, we report on RLSO:Eu²⁺ as next-generation narrow-band green emitter; however, it still faces several technological limitations including low quantum efficiency and poor chemical stability. In this work, by introducing one Na cation into RLSO to replace one Li cation, we synthesized RbNa(Li₃SiO₄)₂:Eu²⁺ (RN:Eu²⁺) phosphor, and [LiO₄] squares in RLSO have been replaced by [NaO₈] cubes in RN via such a polyhedron transformation. Compared with the emission peak of RLSO:Eu²⁺ phosphor, RN:Eu²⁺ also exhibits a narrow-band (FWHM = 41 nm) green emission peaking at 523 nm, and the PL spectrum shows a blue shift, which is ascribed to the Stokes shift effect. More importantly, the substitution of Na can also help to enhance the chemical stability of this compound. By combining the green-emitting RN:Eu²⁺ phosphor, the commercial red-emitting K₂SiF₆:Mn⁴⁺, and blue-emitting InGaN chips ($\lambda_{em} = 455$ nm), high luminous efficacy (111.08 lm W⁻¹) and wide-color-gamut (113% NTSC) white LEDs were obtained. A prototype LCD screen was also manufactured by integrating this kind of wLEDs. These results indicate that the RN:Eu²⁺ phosphor is a promising narrow-band green-emitting candidate for application in backlights of LCDs.

also basically the same as RLSO. Both of them belong to monoclinic structure with space group of *C2/m* and have the same degree of condensation $\kappa = 1$ (Li₃Si:O₄ = 1).^[9b] Figure 1a clearly demonstrates the comparison of the crystal structure diagrams of RLSO and RN, in which RN can be treated as the Li atoms in ring channels of RLSO replaced by Na atoms. In RLSO, the Li3 (2b) and Li4 (2a) sites, which lie on *b*-axis, form LiO₄ squares without contact with each other. The Na addition enables the deletion of these two Li sites; however, Na does not prefer these Li sites. Instead, the Na ions occupy 4g site with local symmetry 2 and form NaO₈ cubes. These cubes are linked with each other by faces and form ...-NaO₈-NaO₈-... column along *b*-axis in RN (Figure 1a). These joints strongly improve the stability of RN compound in comparison with RLSO. Strictly speaking, both compounds are not isotypic because the Li3 (2b) and Li4 (2a) sites do not coincide with Na (4g) sites. Anyway, they have similar cell parameters, the same space group *C2/m*, and most of ions, besides Li3, Li4, and Na, are placed in the same Wyckoff sites. Therefore, the general structural motifs of these

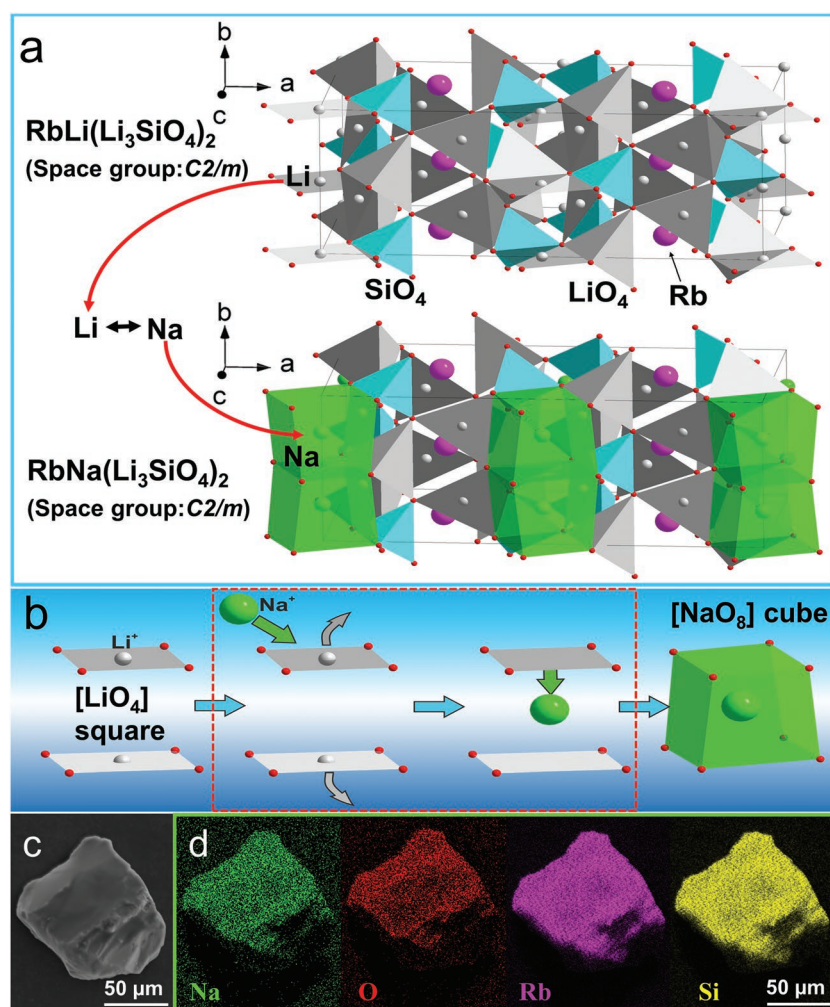


Figure 1. a) Comparison of the crystal structures of RLSO and RN. b) The proposed structural transformation mechanism demonstrating the formation of [NaO₈] cube in RN compared to [LiO₄] square in RLSO due to the bigger ion radii of Na⁺ in comparison with Li⁺. c) SEM image of a typical single RN:Eu²⁺ microcrystal particle. d) Element-mapping images of Rb, Na, Si, and O for the selected RN:Eu²⁺ particle.

2. Result and Discussion

The crystal structure of RN has been previously reported by Hoppe in 1994,^[11] which is

structures are close. The bigger ion radius of Na ion in comparison with Li ion is the reason of structural differences. As given in Figure 1b, the proposed structural transformation process has been demonstrated in the red dotted square, in which the Na ion cannot penetrate to the center of square O_4 and moves out from this center forming coordination with eight O ions with much stronger bonding than coordination of Li with four O ions. Considering the two end members, the polyhedron transformation appears from $[LiO_4]$ squares in RLSO to $[NaO_8]$ cubes in RN. Accordingly, such a variation in the local structure can also affect the emission peak position when doped with Eu^{2+} , as discussed below. More importantly, the chemical stability can be improved for such a compositional variation and the modified local environment effects. Moreover, the XRD pattern of the as prepared RN: Eu^{2+} sample is shown in Figure S1a (Supporting Information), and almost all peaks can be well matched with the simulated pattern of the structure from the ICSD Collection Code 74866. Hence, we also performed the Rietveld refinement using the previously reported crystal structure of RN as the starting model. The refinement result shows that this phosphor has a monoclinic unit cell of $a = 15.7163(3) \text{ \AA}$, $b = 6.3148(2) \text{ \AA}$, $c = 7.8043(1) \text{ \AA}$, $\beta = 90.5720(8)^\circ$, and $V = 774.50(3) \text{ \AA}^3$ with the $C2/m$ space group, which is in agreement with the previous literature.^[11] Detailed information of the refinement processing is provided in Supporting Information (Figure S1b, Table S1, Supporting Information).

To characterize the morphology, elemental composition, and uniformity of RN: Eu^{2+} phosphor, scan electron microscope (SEM) and energy-dispersive X-ray spectroscopy (EDS) were carried out. Figure 1c depicts the SEM image of single RN: Eu^{2+} microcrystal, and the smooth surface of $\approx 100 \mu\text{m}$ particle demonstrates that the microcrystal has a high degree of crystallinity. The element-mapping images of Na, O, Rb, and Si (Figure 1d) indicate that these elements are very homogeneously dispersed within the phosphor particle. Moreover, the uniform Na element distribution further supports that it really penetrates to the RN structure and the removal of $[LiO_4]$ square in RLSO can help to the performance modification.

The photoluminescence (PL) spectra of RN: xEu^{2+} ($x = 1\text{--}15\%$) and the variation of peak wavelength and FWHM with increasing Eu^{2+} doping concentration are shown in Figure S2 (Supporting Information), and the optimal Eu^{2+} concentration is found to be 8%. Figure 2a shows the PL and photoluminescence excitation (PLE) spectra of RN:8% Eu^{2+} . Under 455 nm blue-light excitation, RN:8% Eu^{2+} shows a narrow-band green emission centered at 523 nm with the FWHM of 41 nm (Figure 2a), and the peak wavelengths and FWHM values depending on different Eu^{2+} doping concentrations keep nearly invariable (Figure S2, Supporting Information). The insets of Figure 2a show the photographs of ungrounded sample and the sample under 365 nm UV lamp. The corresponding PLE spectrum of RN:8% Eu^{2+} monitored at 523 nm exhibits a broad

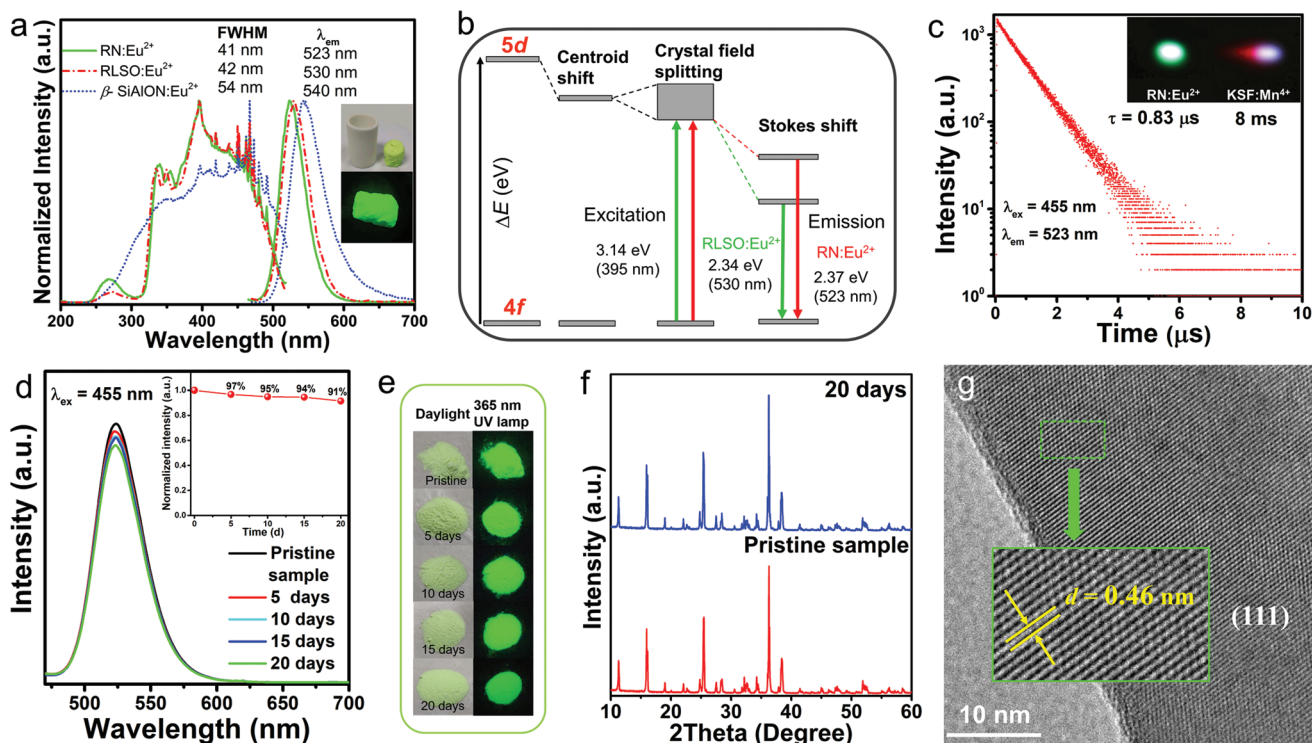


Figure 2. a) PLE and PL spectra of RN:8% Eu^{2+} , RLSO:8% Eu^{2+} (red dotted line), and β -SiAlON: Eu^{2+} (blue short dotted line). The insets show the digital photographs of ungrounded green RN:8% Eu^{2+} phosphor and the phosphor under 365 nm UV lamp, and the size of crucible is 11×20 mm. b) Schematic energy level diagram for Eu^{2+} ions in the RLSO and RN crystal structure. c) The decay curve of RN:8% Eu^{2+} under excitation at 455 nm, monitored at 523 nm; the insets show the images of RN: Eu^{2+} and KSF: Mn^{4+} with the same mobile excitation source. d) PL spectra of the pristine RN: Eu^{2+} and the sample exposed to ambient atmosphere for different days, and the inset shows the dependence of normalized integrated PL intensities on the time. e) The digital photographs of the sample exposed for different times under daylight and 365 nm UV lamp. f) The XRD comparison of pristine sample and the sample exposed for 20 d. g) HRTEM image and the marked lattice fringe of RN:8% Eu^{2+} exposed for 20 d.

band from 300 to 500 nm, indicating that it can be excited by UV to blue light. Furthermore, we measured the low-temperature PL and PLE spectra of RN:8%Eu²⁺ (Figure S3, Supporting Information). Compared with room temperature spectra, the PL spectrum at 80 K has a narrower emission band without obvious shape difference, indicating that this emission peak arises from Eu²⁺ in one site. Considering that the radii of Eu²⁺ ions are between Na⁺ ions and Rb⁺ ions ($R(\text{Na}^+) < R(\text{Eu}^{2+}) < R(\text{Rb}^+)$), one can conclude that the Eu²⁺ ions occupy Rb sites, along with the vacancy-assisted substitution model for the charge balance. Thus, as the charge of Eu²⁺ cannot be compensated by O²⁻ anions in such a rigid structure, the reasonable model is to form Rb⁺ vacancy (V_{Rb}): $2\text{Rb}^+ \leftrightarrow \text{Eu}^{2+} + V_{\text{Rb}}$, as also discussed in the previous literature.^[9b] The smaller cell volume of Eu²⁺-doped compound under investigation (774.50 (3) Å³) in comparison with host material (774.81 Å³) also proves our strategy about Rb ↔ Eu displacement mechanism.

The PL and PLE spectra of the commercial β-SiAlON:Eu²⁺ (Figure 2a, blue short dotted line) and RLSO:8%Eu²⁺ (Figure 2a, red dotted line) are provided as references to compare the optical performance. The PLE spectra of RLSO:8%Eu²⁺ and the commercial β-SiAlON:Eu²⁺ show broad excitation band range from UV to blue region, similar as that of RN:Eu²⁺. As for the difference of the PL spectra, on the one hand, compared with β-SiAlON:Eu²⁺, RN:8%Eu²⁺ has a narrower emission band (FWHM = 41 nm) and a more proper emission peak (523 nm). On the other hand, there are comparable FWHM values between RLSO:8%Eu²⁺ and RN:8%Eu²⁺; however, the Stokes shift of RN:8%Eu²⁺ is obviously smaller than that of RLSO:8%Eu²⁺. The Stokes shift originates from the surrounding lattice relaxation due to the coupling of the 5d electron with the lattice phonons upon the excitation of Eu²⁺ from 4f to the 5d.^[12] Compared with RLSO, the structure of RN is more compact, which leads to the decreased lattice relaxation. Thus, a reduced Stokes shift can be realized for RN:Eu²⁺, suggesting that it may be beneficial to the high-photoluminescence quantum efficiency (QE), as we have compared below. Accordingly, all these differences can be expressed by Commission Internationale de L'Éclairage (CIE) coordinates, and the CIE coordinates of RN:8%Eu²⁺ and β-SiAlON:Eu²⁺ are determined to be (0.2023, 0.7175) and (0.3589, 0.6223), respectively. RN:Eu²⁺ is located at deep green region, which helps to get a larger color gamut than β-SiAlON:Eu²⁺ for LCD backlights. Compared with that of RLSO:8%Eu²⁺, the peak wavelength of RN:8%Eu²⁺ has a 7 nm blue shift besides the slight difference of FWHM. Because the emission band is determined by the 5d level and Stokes shift, we compared the Stokes shift and 5d level of the two compounds. As shown in Figure 2a, the excitation spectrum of RN:8%Eu²⁺ is almost unchanged compared with RLSO:8%Eu²⁺, so the 5d level of RN:8%Eu²⁺ and RLSO:8%Eu²⁺ are basically the same. The calculated Stokes shift of RN:8%Eu²⁺ (1680 cm⁻¹) is smaller than the Stokes shift of RLSO:8%Eu²⁺ (2032 cm⁻¹), therefore, the blue shift is attributed to the reduced Stokes shift, which also helps to realize the high QE. Figure 2b clearly demonstrates the process for the variation of the PL spectra. Under 455 nm excitation, the internal/external quantum efficiency (IQE/EQE) of green phosphor RN:8%Eu²⁺ is 96.2%/44.2%. The EQE of RN:8%Eu²⁺ reaches almost 70% of β-SiAlON:Eu²⁺ (EQE = 64.5%), and is higher

than that of RLSO:8%Eu²⁺ (EQE = 29%),^[9b] and the measurement details are shown in Figure S4 (Supporting Information).

The decay behavior of Eu²⁺ emission at 523 nm for RN:8%Eu²⁺ under 455 nm excitation was measured and shown in Figure 2c. This curve can be well fitted by a single exponential function expressed as follows^[13]

$$I(t) = I_0 + A \exp(-t/\tau) \quad (1)$$

where I and I_0 are the luminescence intensity at time t and $t \gg \tau$, respectively, A is a constant, and τ is the decay time for an exponential component. The calculated lifetime of RN:8%Eu²⁺ is 0.83 μs, and such a single exponential also verifies the single Eu²⁺ emission center at Rb site, which is consistent with the result of the PL spectrum, as also observed in RLSO:Eu²⁺.^[9b] Moreover, for phosphors applied to LCD display, short decay time can effectively avoid ghost signal when we watch high-dynamic video and high-definition programs. The insets of Figure 2c demonstrate the optical decay images upon the same mobile excitation source, showing the difference between RN:Eu²⁺ and KSF:Mn⁴⁺ with ms-level decay time. In such a case, RN:Eu²⁺ has no trailing, thus RN:Eu²⁺ is suitable for LCD backlight application, which should be superior than that of the Mn²⁺-based narrow-band green phosphors.

Figure 2d shows the emission spectra of the pristine RN:8%Eu²⁺ and the sample exposed to ambient atmosphere for different days. The inset of Figure 2d shows that the integrated emission intensities of the sample drop to 97%, 95%, 94%, and 91% of that of the pristine sample after exposure to ambient atmosphere for 5, 10, 15, and 20 d. Hence, the chemical stability of RN:8%Eu²⁺ is better than RLSO:8%Eu²⁺ (74% @7 d), which is attributed to the replacement of [LiO₄] square in RLSO by [NaO₈] cube in RN. The digital photographs of the sample under daylight and 365 nm UV lamp are provided in Figure 2e. In addition, the XRD pattern of the sample after exposed for 20 d is unchanged compared with the pristine sample (Figure 2f). Furthermore, high-resolution transmission electron microscope (HRTEM) analysis was carried out to identify the phase of 20 d exposure sample. It can be found that the continuous lattice fringe measurements with d spacing of 0.46 nm could be assigned to the corresponding (111) plane of RN (Figure 2g), suggesting the high crystalline behavior and stability. In addition, 80 °C/80% relative humidity (RH) test was further performed to evaluate the chemical stability of RN:8%Eu²⁺ at the extreme environmental condition. Figure S5a (Supporting Information) shows the PL spectra of the pristine RN:8%Eu²⁺ and the sample treated in degradation at 80 °C/80% RH for different times, respectively. The inset of Figure S5a (Supporting Information) shows the dependence of normalized integrated PL intensities of RN:8%Eu²⁺ on the time and the degradation data of RLSO:8%Eu²⁺ are also provided as a reference. The integrated emission intensity drops to 59.6% of that of pristine sample after 1 h, which is better than RLSO:8%Eu²⁺ (13% @1 h). The corresponding digital photographs of RN:8%Eu²⁺ sample exposed to 80 °C/80% RH environment for different times were provided in Figure S5b (Supporting Information).

Thermal stability plays an important role in the practical application in white LEDs.^[14] Accordingly, we measured temperature-dependent emission spectra of RN:8%Eu²⁺ from

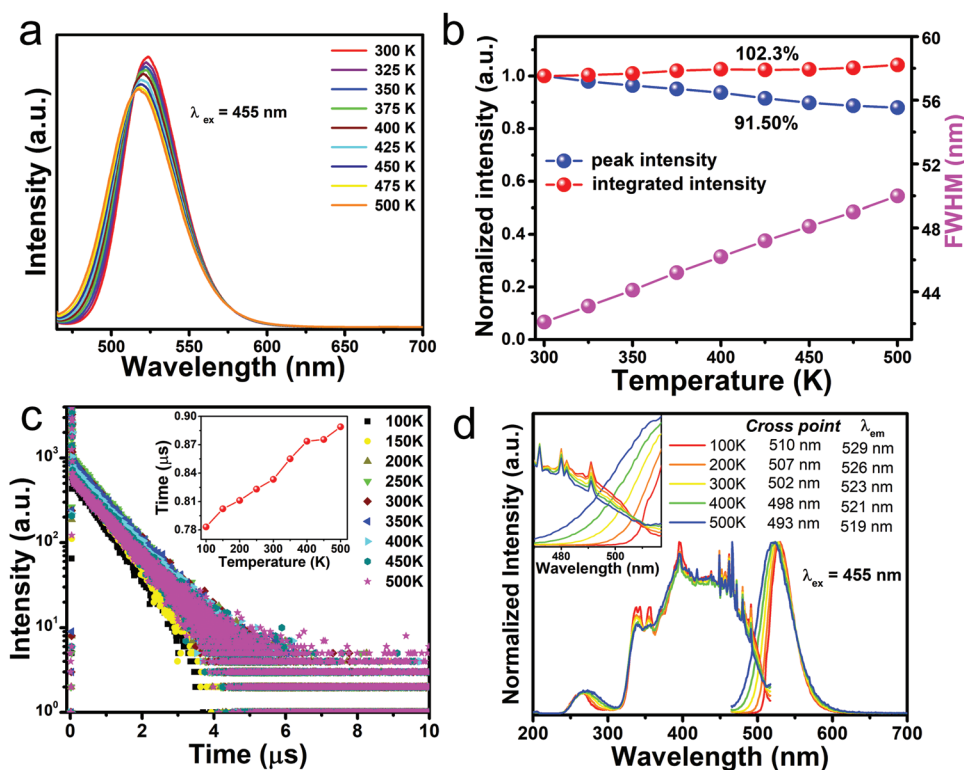


Figure 3. a) Temperature-dependent emission spectra of RN:8%Eu²⁺ phosphor under 455 nm excitation in the temperature range 300–500 K with a temperature interval of 25 K. b) Normalized integrated intensities, peak intensities, and the variation of FWHM of RN:8%Eu²⁺ depending on increasing temperature. c) Decay curves under 455 nm excitation in the temperature range 100–500 K with a temperature interval of 50 K, and the inset shows the lifetimes at different temperatures. d) Temperature-dependent PL (λ_{ex} = 455 nm) and PLE in the temperature range 100–500 K with a temperature interval of 100 K, and the inset shows the overlap region of PL and PLE.

300 to 500 K with a temperature interval of 25 K. As can be seen from **Figure 3a**, under 455 nm excitation, RN:8%Eu²⁺ shows excellent thermal stability and a slight blue shift from 523 to 519 nm with the temperature increasing. Compared with the initial intensity at 300 K, the peak intensity drops only 8.5% at 425 K; even at 500 K, the peak intensity is still about 88% of that at 300 K. The integrated intensity does not show any decrease when the temperature increased to 500 K, which can be ascribed to the emission band broadening (FWHM increasing from 41 to 51 nm, **Figure 3b**). With the temperature increasing from room temperature (300 K) to 425 K, the CIE chromaticity coordinate of RN:8%Eu²⁺ shifts from (0.2023, 0.7175) to (0.1959, 0.6934), indicating that the RN:8%Eu²⁺ shows a moderate chromaticity stability. To better understand how temperature affects luminescence property of RN:8%Eu²⁺, temperature-dependent decay curves monitored at emission peak, high-energy tail, and low-energy tail (12% of the peak intensity) were collected from 100 to 500 K. Normally, as quenching sets in, the luminescence lifetime shortens because of an additional nonradiative contribution to the decay process.^[15] Interestingly, the RN:8%Eu²⁺ shows a different phenomenon. With rising temperature, the lifetime increases from 0.78 to 0.88 μ s (**Figure 3c**) and the lifetimes monitored at the high- and low-energy tails also increase. Moreover, the lifetimes monitored at low-energy tail are longer than monitored at high-energy tail (**Figure S6**, Supporting Information). These observations can be explained by reabsorption. As shown in **Figure 3d**, with the increase of temperature,

the excitation spectra just have a slight change, but the emission spectra broaden so much. Therefore, the overlap or reabsorption region extends, which causes increasing lifetime for RN:8%Eu²⁺ sample with rising temperature. And the reabsorption region of high-energy tail is much smaller than low-energy tail, so the lifetimes monitored at high-energy tail are shorter than monitored at low-energy tail.

Considering of the excellent thermal stability and narrow-band green emission of RN:Eu²⁺, it can be a desirable candidate for LCD backlights. Therefore, we fabricated wLEDs by combining the green phosphor RN:Eu²⁺, the commercial red phosphor KSF:Mn⁴⁺, and blue-emitting InGaN chips (λ_{em} = 455 nm). The emission spectra of the fabricated wLED and the as-fabricated and lightened white LED are shown in **Figure 4a**. Under a current of 20 mA, the optimized wLED device shows a bright white light with a high luminous efficacy up to 111.08 lm W⁻¹ and a wide color gamut of 113% NTSC which is equivalent to 84.5% Rec. 2020 color gamut (**Figure 4b**). And the color space of this wLED is higher than other previous reported phosphor-converted wLEDs (**Table 1**), except for the recently reported Sr₂MgAl₂₂O₃₆:Mn²⁺-based wLED. The correlated color temperature (CCT) and the CIE color coordinate of this wLED are 5196 K and (0.3393, 0.3372), respectively. Furthermore, a 20.5 in. LCD screen was successfully demonstrated by utilizing a backlight with 33 RN:Eu²⁺-based wLEDs. **Figure 4c** illustrates the configuration of this LCD prototype, **Figure 4d** shows the photographs of the prepared and lightened wLEDs,

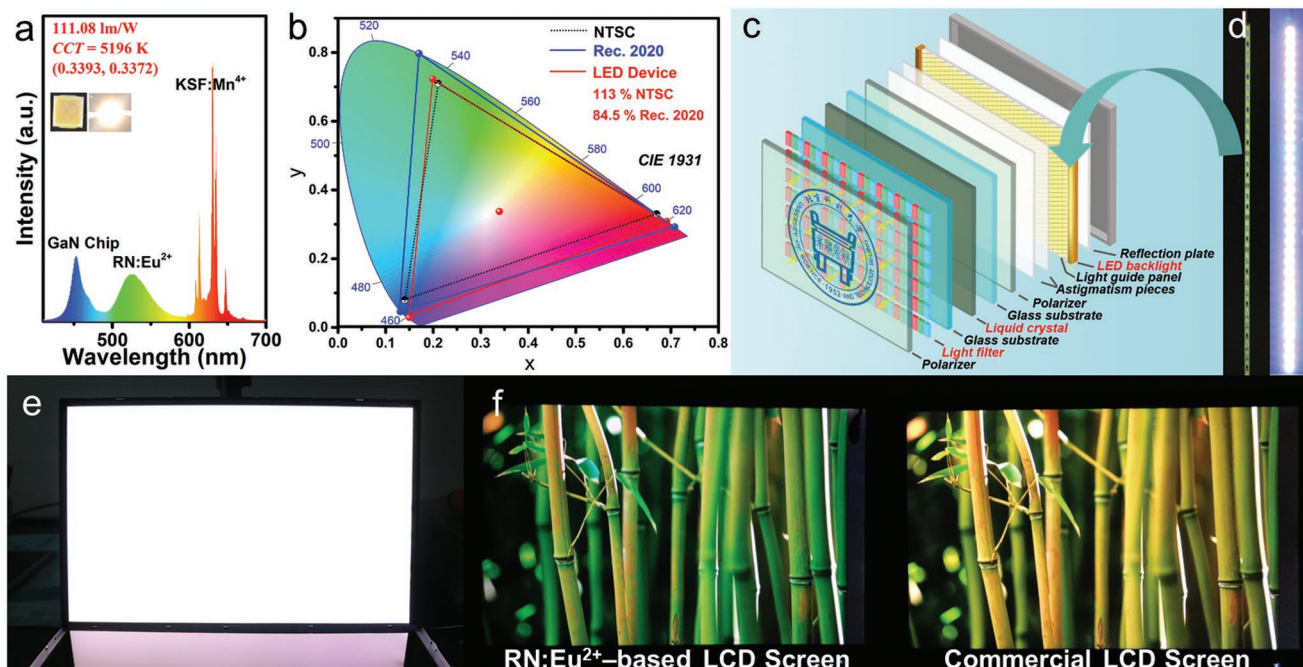


Figure 4. a) Emission spectrum of the wLED device fabricated with the green phosphor RN:Eu²⁺, red phosphor KSF:Mn⁴⁺, and a blue InGaN chip ($\lambda_{em} = 455$ nm) under a current of 20 mA. The insets show the photographs of as-fabricated and lightened wLED. b) CIE 1931 color coordinate of the fabricated wLED, color space of NTSC standard (short dotted line), Rec. 2020 standard (blue line), wLED device (red line). c) Schematic diagram of the configuration of the LCD prototype based on the pc-LEDs technique. d) The as-fabricated and lightened wLEDs backlight. e) The backlight panel of the LCD. f) Comparison of the display images of the RN:Eu²⁺-based LCD screen and commercial LCD screen with the backlight fabricated by blue chips, yellow Y₃Al₅O₁₂:Ce³⁺, and red K₂SiF₆:Mn⁴⁺ phosphors.

and Figure 4e is the backlight panel. With a wider color gamut backlight, the RN:Eu²⁺-based LCD screen can display a more vivid picture (Figure 4f, left) than the commercial LCD screen in which wLEDs are fabricated by blue chips, Y₃Al₅O₁₂:Ce³⁺ (YAG:Ce), and KSF:Mn⁴⁺ (Figure 4f, right). These results take us one step closer toward developing RN:Eu²⁺ phosphor specially tailored for high-performance display applications.

3. Conclusion

In summary, we successfully developed a highly stable new narrow-band phosphor RN:Eu²⁺, which presents a green

Table 1. The comparison of various phosphor-converted white LEDs as LCD backlights.

Phosphor	Color gamut (% NTSC CIE1931)	Reference
Green	Red	
β -SiAlON:Eu ²⁺	CaAlSiN ₃ :Eu ²⁺	82.1 [16]
Sr-SiAlON:Eu ²⁺	CaAlSiN ₃ :Eu ²⁺	83.8 [17]
SrGa ₂ S ₄ :Eu ²⁺	KSF:Mn ⁴⁺	86.4 [18]
Sharp β -SiAlON:Eu ²⁺	KSF:Mn ⁴⁺	96 [6]
γ -AlON:Mn ²⁺ , Mg ²⁺	KSF:Mn ⁴⁺	102.4 [7a]
RLSO:Eu ²⁺	KSF:Mn ⁴⁺	107 [9b]
Sr ₂ MgAl ₂₂ O ₃₆ :Mn ²⁺	KSF:Mn ⁴⁺	127 [7b]
RN:Eu ²⁺	KSF:Mn ⁴⁺	113 This work

emission with $\lambda_{em} = 523$ nm, FWHM = 41 nm, and very low thermal quenching. Thanks to the polyhedra transformation from [LiO₄] squares in RLSO to [NaO₈] cubes in RN, the blue shift of the emission spectrum is attributed to the decreased Stokes shift, and this RN:8%Eu²⁺ green phosphor shows a high external quantum efficiency up to 44.2% and a better chemical stability than that of RLSO:Eu²⁺. By combining RN:Eu²⁺, commercial red phosphor KSF:Mn⁴⁺, and blue InGaN chips, wLEDs are fabricated to serve as backlights. The optimum wLED shows a high luminous efficacy of 111.08 lm W⁻¹ and wide color gamut of 113% NTSC. Furthermore, these wLEDs were integrated to a 20.5 in. LCD screen to demonstrate excellent color reproducibility. Such an inspiring breakthrough in highly stable narrow-band green phosphors represents important steps toward emerging new materials and thus paving new roads to wide-color-gamut LCD technique.

4. Experimental Section

Materials and Preparation: The powder samples of RN:8%Eu²⁺ were synthesized by a solid-state reaction with stoichiometric amount of Rb₂CO₃ (99%, Aladdin), Li₂CO₃ (99.99%, Aladdin), Na₂CO₃ (99.99%, Aladdin), SiO₂ (99.99%, Aladdin), and Eu₂O₃ (99.99%, Aladdin). The molar ratio of Rb₂CO₃, Li₂CO₃, Na₂CO₃, SiO₂, and Eu₂O₃ used in the synthesis was 0.84:6:1:4:0.08. In a typical procedure, 0.194 g Rb₂CO₃, 0.443 g Li₂CO₃, 0.106 g Na₂CO₃, 0.24 g SiO₂, and 0.028 g Eu₂O₃ were weighed and mixed, and then all the starting materials were thoroughly ground in an agate mortar, filled in an alumina crucible and sintered in air at 550 °C for 5 h. After that, the sample was grounded and sintered

several times at 750 °C for 4 h under a reducing atmosphere of N₂–H₂ (20%). Then one can get the sample after reground for further analysis.

Characterization: Structural characterization was conducted by using powder X-ray diffraction (XRD) recorded on a D8 Advance diffractometer (Bruker Corporation, Germany) operating at 40 kV and 40 mA with Cu K_α radiation ($\lambda = 1.5406 \text{ \AA}$). The morphology and particle size of the powder sample were characterized by scanning electron microscope (SEM, JEOL JSM-6510). A JEM-2010 microscope operated at 200 keV was used to record the transmission electron microscope (TEM) images, which were recorded on the 200-mesh carbon-coated nickel grids. The room-temperature photoluminescence (PL) and photoluminescence excitation (PLE) spectra were carried out in an FLS920 fluorescence spectrophotometer (Edinburgh Instruments Ltd., UK) with the Xe900 lamp as the excitation source. The same instrument obtained the decay data with an nF900 lamp used as the excitation source. Temperature-dependent PL spectrum measurements were conducted by a fluorescence spectrophotometer (F-4600, HITACHI, Japan), and the phosphor powders were heated to 500 K in a 25 K interval at a heating rate of 100 K min⁻¹ and held at each temperature for 10 min for thermal equilibrium. The PL and PLE spectra at different temperatures were measured in the FLS920 and the sample was cooled in a liquid nitrogen cryostat on Oxford Instruments that was attached to the FLS920; these instruments also collected temperature-dependent decay data and the phosphor was heated from 100 to 500 K with a 50 K interval at a heating rate of 50 K min⁻¹ and held at each temperature for 10 min for thermal equilibrium.

WLEDs and LCD Screen Fabrication: The wLEDs were fabricated by integrating the green phosphor RN:Eu²⁺, the commercial red phosphor KSF:Mn⁴⁺, and blue LED InGaN chips ($\lambda_{em} = 455 \text{ nm}$). The phosphors were thoroughly mixed with epoxy resin, and the obtained mixture was coated on the LED chips. The photoelectric properties, including the emission spectrum, color temperature (CCT), color rendering index (R_a), and CIE color coordinate of the LED, were collected by using an integrating sphere spectroradiometer system (ATA-1000, Ever fine).

Supporting Information

Supporting Information is available from the Wiley Online Library or from the author.

Acknowledgements

H.X.L., M.Z., and Y.Y.Z. contributed equally to this work. The present work was supported by the National Natural Science Foundations of China (Grant Nos. 51722202, 91622125, and 51572023), Natural Science Foundations of Beijing (2172036), Fundamental Research Funds for the Central Universities (FRF-TP-18-002C1), and the Guangdong Provincial Science & Technology Project (No. 2018A050506004).

Conflict of Interest

The authors declare no conflict of interest.

Keywords

light-emitting diodes, phosphor, photoluminescence

Received: March 7, 2019

Revised: May 8, 2019

Published online:

- [1] a) P. Pust, V. Weiler, C. Hecht, A. Tucks, A. S. Wochnik, A. K. Henss, D. Wiechert, C. Scheu, P. J. Schmidt, W. Schnick, *Nat. Mater.* **2014**, *13*, 891; b) H. W. Chen, J. H. Lee, B. Y. Lin, S. Chen, S. T. Wu, *Light: Sci. Appl.* **2018**, *7*, 17168.
- [2] a) T. H. Kim, K. S. Cho, E. K. Lee, S. J. Lee, J. Chae, J. W. Kim, D. H. Kim, J. Y. Kwon, G. Amaratunga, S. Y. Lee, B. L. Choi, Y. Kuk, J. M. Kim, K. Kim, *Nat. Photonics* **2011**, *5*, 176; b) H. V. Han, H. Y. Lin, C. C. Lin, W. C. Chong, J. R. Li, K. J. Chen, P. Yu, T. M. Chen, H. M. Chen, K. M. Lau, H. C. Kuo, *Opt. Express* **2015**, *23*, 32504; c) S. Reineke, *Nat. Mater.* **2015**, *14*, 459.
- [3] a) L. Wang, X. Wang, T. Kohsei, K. Yoshimura, M. Izumi, N. Hirotsaki, R. J. Xie, *Opt. Express* **2015**, *23*, 28707; b) S. X. Li, R. J. Xie, T. Takeda, N. Hirotsaki, *ECS J. Solid State Sci. Technol.* **2018**, *7*, R3064.
- [4] P. Pust, P. J. Schmidt, W. Schnick, *Nat. Mater.* **2015**, *14*, 454.
- [5] a) E. Jang, S. Jun, H. Jang, J. Lim, B. Kim, Y. Kim, *Adv. Mater.* **2010**, *22*, 3076; b) Y. Wei, Z. Y. Cheng, J. Lin, *Chem. Soc. Rev.* **2019**, *48*, 310; c) Y. Shirasaki, G. J. Supran, M. G. Bawendi, V. Bulović, *Nat. Photonics* **2013**, *7*, 13.
- [6] S. X. Li, L. Wang, D. Tang, Y. J. Cho, X. J. Liu, X. T. Zhou, L. Lu, L. Zhang, T. Takeda, N. Hirotsaki, R. J. Xie, *Chem. Mater.* **2018**, *30*, 494.
- [7] a) K. Yoshimura, H. Fukunaga, M. Izumi, K. Takahashi, R. J. Xie, N. Hirotsaki, *Jpn. J. Appl. Phys.* **2017**, *56*, 041701; b) Y. L. Zhu, Y. J. Liang, S. Q. Liu, H. R. Li, J. H. Chen, *Adv. Opt. Mater.* **2019**, *7*, 1801419.
- [8] a) Z. G. Xia, Q. L. Liu, *Prog. Mater. Sci.* **2016**, *84*, 59; b) Z. G. Xia, Z. H. Xu, M. Y. Chen, Q. L. Liu, *Dalton Trans.* **2016**, *45*, 11214; c) H. X. Liao, M. Zhao, M. S. Molokeev, Q. L. Liu, Z. G. Xia, *Angew. Chem., Int. Ed.* **2018**, *57*, 11728; d) J. W. Qiao, L. X. Ning, M. S. Molokeev, Y. C. Chuang, Q. L. Liu, Z. G. Xia, *J. Am. Chem. Soc.* **2018**, *140*, 9730; e) Z. C. Zhang, C. G. Ma, R. Gautier, M. S. Molokeev, Q. L. Liu, Z. G. Xia, *Adv. Funct. Mater.* **2018**, *28*, 1804150.
- [9] a) D. Dutzler, M. Seibald, D. Baumann, H. Huppertz, *Angew. Chem., Int. Ed.* **2018**, *57*, 13676; b) M. Zhao, H. X. Liao, L. X. Ning, Q. Y. Zhang, Q. L. Liu, Z. G. Xia, *Adv. Mater.* **2018**, *30*, 1802489; c) M. Zhao, Y. Y. Zhou, M. S. Molokeev, Q. Y. Zhang, Q. L. Liu, Z. G. Xia, *Adv. Opt. Mater.* **2019**, *7*, 1801631; d) A. Meijerink, *Sci. China Mater.* **2019**, *62*, 146.
- [10] a) M. Seibald, D. Baumann, T. Fiedler, S. Lange, H. Huppertz, D. Dutzler, T. Schroder, D. Bichler, G. Plundrich, S. Peschke, H. Gregor, G. Achrainger, K. Wurst, WO2018029304 A1, **2018**; b) M.-H. Fang, J. L. Leañor Jr, R.-S. Liu, *ACS Energy Lett.* **2018**, *3*, 2573.
- [11] J. Hoffmann, R. Brandes, R. Hoppe, *Z. Anorg. Allg. Chem.* **1994**, *620*, 1495.
- [12] P. Dorenbos, *J. Lumin.* **2000**, *91*, 155.
- [13] G. Blasse, B. Grabmaier, *Luminescent Materials*, Springer, Berlin **1994**.
- [14] a) Y. H. Kim, P. Arunkumar, B. Y. Kim, S. Unithrattil, E. Kim, S. H. Moon, J. Y. Hyun, K. H. Kim, D. Lee, J. S. Lee, W. B. Im, *Nat. Mater.* **2017**, *16*, 543; b) P. F. Smet, J. J. Joos, *Nat. Mater.* **2017**, *16*, 500.
- [15] V. Bachmann, C. Ronda, A. Meijerink, *Chem. Mater.* **2009**, *21*, 2077.
- [16] R. J. Xie, N. Hirotsaki, T. Takeda, *Appl. Phys. Express* **2009**, *2*, 022401.
- [17] Y. Fukuda, N. Matsuda, A. Okada, I. Mitsuishi, *Jpn. J. Appl. Phys.* **2012**, *51*, 122101.
- [18] J. H. Oh, H. Kang, M. Ko, Y. R. Do, *Opt. Express* **2015**, *23*, A791.